UNIVERSITY OF DUNDEE

University of Dundee

Trypanosoma cruzi phosphomannomutase and guanosine diphosphate-mannose pyrophosphorylase ligandability assessment

Zmuda, Filip; Shepherd, Sharon M.; Ferguson, Michael A. J.; Gray, David W.; Torrie, Leah S.; De Rycker, Manu

Link to publication in Discovery Research Portal

1   **Title**

2   *Trypanosoma cruzi* **phosphomannomutase and guanosine diphosphate-mannose**

3   **pyrophosphorylase ligandability assessment.**

4   **Running title**

5   *T. cruzi* **PMM and GDP-MP ligandability assessment.**

6

7   *Filip Zmuda*[a], *Sharon M. Shepherd*[b], *Michael A. J. Ferguson*[a], *David. W. Gray*[a#], *Leah S. Torrie* [a],

8   *Manu De Rycker*[a#]

9   [a]Drug Discovery Unit, Wellcome Centre for Anti-Infectives Research, School of Life Sciences,

10   University of Dundee, Dow Street, Dundee DD1 5EH, United Kingdom.

11   [b]Protein Production Team, Wellcome Centre for Anti-Infectives Research, School of Life Sciences,

12   University of Dundee, Dow Street, Dundee DD1 5EH, United Kingdom.

13

14   *Correspondent footnote:*

15   [#]E-mail: d.w.gray@dundee.ac.uk. Phone: +44 (0) 1382 386247

16   [#]E-mail: m.derycker@dundee.ac.uk. Phone: +44 (0) 1382 386211

17

18   **Abstract**

19   Chagas' disease, which is caused by the *Trypanosoma cruzi* parasite, has become a global health

20   problem that is currently treated with poorly tolerated drugs that require prolonged dosing. Therefore,

21   there is a clinical need for new therapeutic agents that can mitigate these issues. The

22   phosphomannomutase (PMM) and guanosine diphosphate-mannose pyrophosphorylase (GDP-MP)

23   enzymes form part of the *de novo* biosynthetic pathway to the nucleotide sugar guanosine

24   diphosphate-mannose. This nucleotide sugar is used either directly, or indirectly via the formation of

25   dolichol-phosphomannose, for the assembly of all mannose-containing glycoconjugates. In *T. cruzi*,

26   mannose-containing glycoconjugates include the cell-surface glycoinositol-phospholipids and the

27   glycosylphosphatidylinositol-anchored mucin-like glycoproteins that dominate the cell surface

28   architectures of all life-cycle stages. This makes PMM and GDP-MP potentially attractive targets for

29   a drug discovery programme against Chagas' disease. To assess the ligandability of these enzymes in

30   *T. cruzi*, we have screened 18,117 structurally diverse compounds exploring drug-like chemical space

31   and 16,845 small polar fragment compounds using an assay interrogating activities of both PMM and

32   GDP-MP enzymes simultaneously. This resulted in 48 small fragment hits, and on re-testing 20 were

33   found to be active against the enzymes. Deconvolution revealed that these were all inhibitors of *T.*

34   *cruzi* GDP-MP, with compounds **2** and **3** acting as uncompetitive and competitive inhibitors,

35   respectively. Based on these findings, the *T. cruzi* PMM and GDP-MP enzymes were deemed not

36   ligandable and poorly ligandable, respectively, using small-molecules from conventional drug

37   discovery chemical space. This presents a significant hurdle to exploiting these enzymes as

38   therapeutic targets for Chagas' disease.

39

40   **<u>Introduction</u>**

41   Chagas' disease is a vector borne disease, caused by the parasite *Trypanosoma cruzi*, with an

42   increasing global health burden due to migration between endemic Latin American and non-endemic

43   countries. This is signified by the estimated 7-8 million people that are infected with *T. cruzi*

44   worldwide, of which 300,000 are estimated to live in the United States and 59,000–108,000 in Europe

45   (1). Infection with *T. cruzi* is first associated with an acute phase that tends to last up to approximately

46   8 weeks and, in most cases, patients present with non-specific symptoms such inflammation at the site

47   of parasite entry and fever. The acute phase usually resolves spontaneously and most patients will

48   enter an indeterminate chronic phase, where infection with *T. cruzi* persists in the absence of clinical

49   symptoms and with good prognosis. However, approximately 30–40% of chronically infected patients

50   will develop cardiac or gastrointestinal organ involvement over time, which can be fatal (2). For the

51 last four decades, treatment of Chagas' disease has been limited to benznidazole and nifurtimox, both

52 of which are nitroheterocyclic drugs (3). Unfortunately, therapeutic failures are commonplace due to

53 the long duration of treatments required with these drugs and their broad side effect profiles (2–3),

54 although the recent BENDITA clinical trial offers promise of a more effective and shorter term

55 treatment regimen (4). Despite this, there is a clear clinical need for new treatments against Chagas'

56 disease that are better tolerated and require shorter dosage regimens. One way to achieve this is

57 through a focused drug-discovery programme targeting a validated biochemical pathway that is

58 essential for parasite viability and/or virulence.

59

60 *T. cruzi* is known to produce an array of mannose-containing glycoconjugates, such as glycoinositol

61 phospholipids (GIPLs) and glycosylphosphatidylinositol (GPI) anchored mucin-like glycoproteins,

62 trans-sialidase enzymes, and other N-glycosylated glycoproteins, which coat the outer surface of the

63 parasite (5–8). Amongst other things, these glycoconjugates play an important role in parasite

64 virulence, and their ability to enter host cells (5–8). Importantly, genetic disruption of the biosynthetic

65 pathway responsible for the production of similar glycoconjugate structures in related trypanosomatid

66 parasites has been shown to be lethal to *T. brucei* (9–12) and to render *Leishmania mexicana* (13–16)

67 and *L. major* (17) either less virulent or completely avirulent. A key intermediate in the production of

68 these glycoconjugate structures is guanosine diphosphate-mannose (GDP-Man), which acts as a donor

69 of activated mannose for glycosylation reactions. GDP-Man is known to be present at low basal levels

70 in *T. cruzi, T. brucei, and L. major*, and this has been linked to the high flux of this substrate in

71 trypanosomatids (6). This, coupled with the above-mentioned genetic findings, highlights the

72 biological importance of GDP-Man in these parasites.

73

74 In eukaryotes, GDP-Man is generated through a series of successive enzymatic reactions, where the

75 penultimate step involves the conversion of mannose-6-phosphate (M-6-P) to mannose-1-phosphate

76 (M-1-P) by the phosphomannomutase (PMM) enzyme through a transfer of a phosphate functionality,

77 made available by the glucose-1,6-bisphosphate (G-1,6-BP) co-factor, from the C-6 position to the C-

78 1 position of the mannose sugar (6, 17). It is important to note that this transformation is not

79 associated with a mass change and cannot be measured directly using standard biochemical

80 approaches in a high-throughput manner. The next step in this pathway involves the addition of M-1-

81 P into the guanosine-monophosphate moiety of guanosine triphosphate (GTP) by the guanosine

82 diphosphate-mannose pyrophosphorylase (GDP-MP) enzyme to produce GDP-Man (6, 18) (Figure 1).

83 Drug discovery efforts utilising high-throughput screening (19) and target-based design (20)

84 approaches have been able to identify a small number of inhibitors of the *L. mexicana* and *L.*

85 *donavani* GDP-MP enzymes that were capable of killing the parasites *in vitro*.

86

87 Collectively, the above findings provide genetic and pharmacological evidence for the GDP-Man

88 biosynthetic pathway as a target for new drugs against *Leishmania* and *T. brucei* parasites. However,

89 the ability of *T. cruzi* PMM and GDP-MP to bind small molecules other than substrates *in vitro*,

90 defined as ligandability (21), remains an open question. In order to address this knowledge gap, we

91 have developed a high-throughput, colourimetric PMM and GDP-MP enzyme assay system to

92 measure the collective output of both enzymes and a GDP-MP assay that measures the output of the

93 single enzyme as a hit de-convolution strategy. Moreover, both assay platforms were further expanded

94 to allow for interrogation of enzyme activities at different substrate concentrations (*i.e.* standard and

95 high-substrate configurations) (Figure 2). These tools were used to screen a subset of our diverse

96 compound libraries and a focused small polar fragment library in an effort to identify chemical matter

97 capable of inhibiting *T. cruzi* PMM and/or GDP-MP, and subsequently further profile the

98 pharmacology of hits of interest. Ultimately, the findings from these studies were used to assess the

99 ligandability of the target *T. cruzi* PMM and GDP-MP enzymes.

100

101

102

4

103

<u>Results</u>

<u>Biochemical assay development.</u>

106 To identify suitable screening substrate concentrations, Michaels-Menten constants (K_m) were

107 acquired for M-1-P and GTP substrates using the GDP-MP assay, followed by M-6-P and G-1,6-BP

108 using the PMM-GDP-MP assay (Figure 3 and Table 1). Multiple configurations of the assays were set

109 up for screening and/or further pharmacological assessment using final substrate concentrations either

110 approximately equivalent to K_m values (standard configuration) or 5 to 10-fold K_m values (high-

111 substrate configurations). Linearity of both the GDP-MP and PMM-GDP-MP assays was investigated

112 using the standard and high-substrate configurations. In the case of the GDP-MP assay, a linear

113 response for up to 50 min ($R^2 = 0.98$ and 0.99 respectively) was observed using both standard and

114 high-substrate configurations (Figure S1a). The PMM-GDP-MP assay biochemical response was

115 associated with an initial lag phase of 30 min for both assay configurations, followed by a subsequent

116 linear response for the remaining 60 min of the standard configuration time course reaction ($R^2 =$

117 0.99). The lag-phase was likely due to the need to build up M-1-P substrate by the PMM enzyme for

118 the successive GDP-MP biochemical reaction. Time-course assay linearity was slightly shorter for the

119 high-substrate assay configuration (i.e. 30–80 min; $R^2 = 0.99$). Finally, as our screening compound

120 libraries are formulated in dimethyl sulfoxide (DMSO), the tolerance of the biochemical assays to this

121 solvent were investigated. Both the GDP-MP and PMM-GDP-MP biochemical assays were shown to

122 be tolerant to DMSO up to 2% v/v (Figure S2).

123

124 The biochemical assays rely on the detection of pyrophosphate using a colourimetric reporter system

125 comprising of a pyrophosphatase enzyme that generates free inorganic phosphate, which in turn reacts

126 with the BIOMOL® Green reagent to generate a quantitative colourimetric response. To identify

127 compounds capable of interfering with the pyrophosphatase and BIOMOL® Green reporter, a counter-

128 screen assay was established looking at this system in isolation. A titration of sodium pyrophosphate

5

129   in the presence of a fixed concentration of pyrophosphatase reporter enzyme, which matched that used

130   for the GDP-MP and PMM-GDP-MP biochemical assays, revealed complete turnover of

131   pyrophosphate in less than one minute (Figure S3a). Importantly, the measured response signal was

132   linear ($R^2 = 0.99$) relative to pyrophosphate concentration (Figure S3b).

133

134   <u>Diversity screening and hit confirmation.</u>

135   Single point screening of a diverse set of 18,117 compounds using the standard configuration PMM-

136   GDP-MP assay platform failed to identify any chemical matter capable of inhibiting the biochemical

137   activity of these enzymes by 30% or more at a compound concentration of 10 μM (Figure 4a).

138   However, screening a compound library comprising 16,845 small polar fragments at a higher

139   compound concentration of 300 μM identified 48 hits at ≥30% inhibition (0.29% hit-rate) (Figure 4b).

140   Mean robust Z' values of 0.87 ± 0.04 (SD; N = 60) and 0.90 ± 0.03 (SD; N = 52) were obtained for

141   the former and latter screens, where a Z' of >0.5 signifies a highly robust biochemical assay (22).

142

143   In order to establish the potency and confirm the presence or absence of technology interference, hit

144   compounds that were available (46 out of the 48) underwent concentration-response assessment using

145   the standard configuration PMM-GDP-MP and reporter counter-screen biochemical assays. Excellent

146   linear correlations were established between the calculated pIC_{50} parameters, defined as $-\log(IC_{50}$

147   (M)), for independent assay replicates (Figures 5a and 5b). Out of the tested initial hit compounds,

148   inhibitory activity (i.e. mean $pIC_{50} \geq 3$ (N = 2)) against the GDP-MP and/or PMM enzymes was

149   established for 20 compounds, while the remaining compounds were either inactive (i.e. 13

150   compounds with mean $pIC_{50} <3$ (N = 2)) or were deemed to be technology interferers (i.e. 13

151   compounds with mean $pIC_{50} \geq 3$ (N = 2) in the counter-screen) (Figure 5c). To deconvolute the

152   enzymatic target of the 20 hits, concentration-response assessment was also performed using the

153   standard configuration GDP-MP enzymatic assay (Figure 6). Out of the 20 hits, compound **1**

154   exhibited much greater potency in both the PMM-GDP-MP and GDP-MP assays compared to the

6

155 remaining compounds (Figure 6 and Table 2). However, this compound has been identified as a hit

156 against a number of other enzymes in our previous screening efforts and was deemed to be a

157 promiscuous inhibitor. Compound **2** appeared to be active in the standard configuration PMM-GDP-

158 MP assay but inactive in the standard configuration GDP-MP assay (Figure 6 and Table 2),

159 suggesting inhibitory activity against the PMM enzyme. To confirm the activity of compounds **2** and

160 **3**, fresh solid material was obtained and both demonstrated activity in the standard and high-substrate

161 configurations of the PMM-GDP-MP assay (Table 2, and Figure S4a and S4c). In line with the poor

162 level of enzyme inhibition, compounds **1**–**4** were inactive in our intracellular *T. cruzi* phenotypic

163 assay (23) at 100 μM. Interestingly, **2** was shown to be inactive against the GDP-MP enzyme when

164 tested using the standard configuration assay, but capable of inhibition when substrate concentrations

165 were increased by 10-fold (i.e. using the high-substrate configuration assay) (Table 2 and Figure S4b),

166 indicative of uncompetitive inhibition. The re-purchased stock of compound **3** was also confirmed to

167 be active in the standard configuration GDP-MP assay (Table 2 and Figure S4d), with an observable

168 shift in the concentration response curve and a subsequent drop in the pIC_{50} parameter when the high-

169 substrate configuration of the assay was used, indicative of competitive inhibition.

170

171 <u>Discussion.</u>

172 With the appropriate biochemical tools in place, we sought to address the knowledge gap of *T. cruzi*

173 PMM and GDP-MP enzyme ligandability. Our initial efforts to identify inhibitors of either the *T.*

174 *cruzi* PMM or the GDP-MP enzymes by performing a screen of 18,117 compounds exploring a

175 diverse range of chemical space using the standard configuration PMM-GDP-MP assay platform were

176 not successful (Figure 4a). On the whole, the active sites of the PMM and GDP-MP enzymes exhibit a

177 high level of homology between species (17, 20, 24) and *Leishmania* GDP-MP enzymes have been

178 found to be ligandable by drug-like compounds. Lackovic *et al* reported an initial hit rate of

179 approximately 0.6% following a screen of approximately 80,000 compounds against *L. major* GDP-

180 MP. Following confirmation and technology interference counter-screening and hit expansion, the

181 authors identified 21 inhibitors with cell-free pIC_{50} values spanning a range of 5.0 to 6.3. The majority

7

182   of these compounds were classified into three distinct chemotypes, namely pyrazolin-3,5-diones, 4-

183   pyrizinylquinolines, and thiadiazole-like compounds (19). In addition to this, Mao *et al* detailed 4

184   further inhibitors with pK_i values ranging from 4.6 to 5.2 against *L. mexicana* and *L. donovani* GDP-

185   MP enzymes (20). None of the previously published compounds were part of the screening sets used

186   here. The screens did include a number of compounds with 4-pyrizinylquinoline and thiadiazole-like

187   cores, which were all inactive in the standard configuration PMM-GDP-MP assay. As no *Leishmania*

188   enzyme data is available for these specific compounds, this information does not provide insight into

189   the differences in ligandability between the *Leishmania* and *T. cruzi* enzymes.

190

191   It is possible that the apparent lower level of ligandability of *T. cruzi* PMM and/or GDP-MP

192   compared to the *Leishmania* enzymes is due to subtle structural differences between the parasite

193   species, which may drive the observed marked differences in the kinetic properties of the different

194   GDP-MP enzymes. Mao *et al* observed that the catalytic efficiency of the *L. mexicana* GDP-MP

195   enzyme for M-1-P and GTP substrates was 10- and 20-fold higher, respectively, than the equivalent *L.*

196   *donovani* enzyme (20). Moreover, our GTP K_m value for *T. cruzi* GDP-MP was 2.4-, 5.3- and 27-fold

197   higher than reported for *L. donavani, L. mexiciana* and *L. major* respectively, while the *T. cruzi* M-1-

198   P K_m parameter value was in line with the reported *Leishmania* K_m values (19–20).

199

200   By taking into account the polar nature of the substrates and/or co-factors for the PMM and GDP-MP

201   enzymes, we attempted to bias our hunt for inhibitors of these *T. cruzi* enzymes by performing a

202   screen using a focused compound library comprising of 16,845 small polar molecules. The use of

203   lower molecular weight compounds for screening campaigns is usually associated with the

204   identification of hits exhibiting weak inhibitory properties, which is an inherent consequence of the

205   reduced number of potential interactions that can take place between a small fragment and the target

206   enzyme (25). With this in mind, compounds from the small polar library were tested at a higher

207   concentration of 300 µM compared to the previously screened compound sets. This endeavour was

8

208 more successful as a small number of hits capable of inhibiting the biochemical response of the *T.*

209 *cruzi* PMM-GDP-MP assay were identified. An initial de-convolution screen using the standard

210 configuration GDP-MP assay showed that the majority of the compounds were also active in this

211 assay, indicating that these were inhibitors of GDP-MP. The exception to this was compound **2** that

212 showed marked activity against the standard configuration PMM-GDP-MP assay, but appeared

213 inactive in the standard configuration GDP-MP deconvolution assay, suggesting that **2** was an

214 inhibitor of the *T. cruzi* PMM enzyme. However, on further concentration-response evaluation,

215 compound **2** was found to display behaviour that is consistent with uncompetitive GDP-MP enzyme

216 inhibition, where the GTP substrate molecule must first be bound to the enzyme to allow binding of

217 the inhibitory compound (26). This is supported by the similar pIC_{50} values obtained for **2** using the

218 standard configuration PMM-GDP-MP and high-substrate configuration GDP-MP assays that both

219 utilised the GTP substrate at saturating concentrations, and the lack of activity in the standard

220 configuration GDP-MP assay where the GTP substrate was used at a concentration approximating its

221 K_m value. In contrast to this, compound **3** exhibited behaviour that was suggestive of competitive

222 inhibition of the *T. cruzi* GDP-MP enzyme, as exemplified by the observable shift in the dose

223 response curve and the corresponding decrease in the pIC_{50} value following a 10-fold increase in

224 biochemical assay substrate concentrations.

225

226 In summary, our inability to identify and confirm a single inhibitor of the *T. cruzi* PMM enzyme from

227 a total of 34,962 compounds exploring both drug-like and small polar compounds suggests that, in

228 this particular chemical space, *T. cruzi* PMM is not ligandable. Moreover, based on criteria reported

229 by Edfeldt *et al* (21), the *T. cruzi* GDP-MP was deemed to be poorly ligandable as only a small

230 number of polar fragment-like hits were identified, which exhibited weak inhibitory properties in our

231 cell free biochemical assays. Therefore, despite genetic and pharmacological evidence for PMM and

232 GDP-MP enzymes as potential therapeutic targets for leishmaniasis, the apparent poor ligandability of

233 the *T. cruzi* variants presents an important hurdle for exploiting these targets for Chagas' disease drug

234 discovery.

9

235

236

237

238

Materials and Methods.

General.

All enzyme and substrate solution dilutions were prepared in assay buffer comprising 25 mM Tris-HCl (pH 7.5), 150 mM NaCl, 4 mM $MgCl_2$, 0.01% v/v Tween 20, and 1 mM dithiothreitol in ultrapure water. Biochemical assays were performed in a 50 µL final assay volume using clear 384-well assay microplates (Greiner; catalogue no. 781101) at room temperature. Unless stated otherwise, all reagent concentrations are written as final biochemical assay concentrations, and DMSO or compounds were added to assay plates using Echo acoustic dispensers (Labcyte, USA). Reagent addition for high-throughput screening assays was performed using an Xrd-384 liquid dispenser (FluidX, UK) and a BioFill Solo/Xrd-384 16 channel resin nozzle (2.00–200 µL) tubing cartridge (FluidX; catalogue no. 34-1005-S). Biochemical reactions were terminated by addition of 50 µL of BIOMOL® Green (Enzo Life Sciences; catalogue no. BML-AK111-1000) reagent, after which absorbance was measured following a 30 minute incubation at room temperature. Absorbance measurements were performed at 650 nm using a PHERAStar microplate reader (BMG Labtech, Germany) and the data are represented as relative absorbance units (RAU). Linear and non-linear regression was performed using the SigmaPlot 12.5 software, unless stated otherwise.

T. cruzi PMM and GDP-MP production and purification.

The genes coding for *T. cruzi* GDP-MP and PMM (UniProtKB Q4CMK4 and Q4E4A3, respectively) were synthesised, followed by optimisation of the codons for *E. coli* by GenScript and cloning into modified pET15b with an N-terminal histidine and maltose-binding protein tag and TEV cleavage site

10

260   for GDP-MP, and an N-terminal histidine tag and TEV cleavage site for PMM. The respective

261   plasmids were transformed into BL21 DE3 *E. coli* cells, and autoinduction media (1 L for GDP-MP

262   and 2 L for PMM) supplemented with AMP was inoculated and grown for 4 hours at 37 °C, followed

263   by a further 17 hours at 20 °C. Cell pellets were generated by centrifugation at 3,500 g for 20 min,

264   and in each case the supernatant was discarded. The pellets were resuspended in 20 mL of lysis buffer

265   (i.e. 25 mM Tris, pH 8.5; 500 mM NaCl; 20 mM imidazole; 1 cOmplete™ Protease Inhibitor Cocktail

266   tablet (Roche, Germany)) and the resulting suspension was then passed through a continuous flow cell

267   disruptor (Constant Systems Ltd., UK) at 30 KPSI. The *T. cruzi* GDP-MP sample was then

268   centrifuged at 37,500 g for 30 min and filtered (0.45 μm), and the PMM sample was centrifuged at

269   40,000 g for 30 min and filtered (0.22 μm).

270

271   To purify the proteins, a 5 mL HisTrap™ Ni HP column (GE Healthcare, USA) was first equilibrated

272   with buffer 'A' (i.e. 25 mM Tris, pH 8.5; 500 mM NaCl; 20 mM imidazole) using an ÄKTA™ pure

273   chromatography system (GE Healthcare, USA) followed by loading of protein sample at 5 mL/min.

274   Next the column was washed with 10 column volumes of buffer 'A', followed by 10 column volumes

275   of 5% v/v buffer 'B' (i.e. 25 mM Tris, pH 8.5; 500 mM NaCl; 0.5 mM TCEP; 500 mM imidazole) to

276   remove histidine-rich contaminating proteins. A gradient of 5% v/v to 50% v/v buffer 'B' was then

277   used to elute the proteins. TEV protease was added to the protein samples (7 mg for GDP-MP and 2

278   mg for PMM), which were then dialysed against buffer 'C' (i.e. 25 mM Tris, pH 7.5; and 250 mM

279   NaCl). The proteins were passed through the 5 mL HisTrap™ Ni HP column (GE Healthcare, USA)

280   to remove the TEV protease and any uncleaved proteins, where cleaved proteins were retained on the

281   column. A gradient of 0% v/v to 50% v/v of buffer 'B' over 10 column volumes was applied to

282   remove the cleaved protein from the histidine and/or maltose binding protein, and TEV. Protein

283   samples were concentrated to 11 mL using 30 kDa cut-off Vivaspin™ protein concentrators

284   (Sartorius, Germany), filtered (0.22 μm), and loaded onto XK26/60 Superdex 200 and 75 columns

285   (GE Healthcare, USA), for GDP-MP and PMM respectively, which were previously equilibrated with

286   buffer 'C'. Protein loading was performed using a 10 mL loop at 1 mL/min. The GDP-MP and PMM

11

287   proteins were eluted using buffer 'C' as hexamers and dimers respectively (columns were calibrated

288   with Bio-Rad (USA) standards). *T. cruzi* GDP-MP was concentrated to 2.49 mg/mL and a total yield

289   of 12 mg was achieved. *T. cruzi* PMM was concentrated to 5.77 mg/mL and a total yield of 3.24 mg

290   was achieved. Mass-spectrometry was used to confirm the identity of the proteins and densitometry

291   (measured using a Bio-Rad imager (Bio-Rad, USA)) was used to confirm that both protein samples

292   exhibited 100% purity.

293   <u>Primary assay development.</u>

294   To calculate the Michaelis constant (K_m) for the M-1-P substrate, 20 minute time-course reactions

295   using a fixed concentration of GDP-MP enzyme (3.13 nM), a saturating concentration of GTP

296   substrate (600 μM) mixed with inorganic pyrophosphatase (1 U/mL; Merck, catalogue no. I5907-

297   1MG), and varying concentrations of M-1-P substrate (150 μM; 75 μM; 37.5 μM; 18.8 μM; 9.38 μM;

298   4.69 μM; and 2.34 μM) were performed. The K_m for the GTP substrate was acquired in a similar

299   manner using a saturating concentration of M-1-P (150 μM) and varying concentrations of GTP

300   substrate (300 μM; 150 μM; 75 μM; 37.5 μM; 18.8 μM; 9.38 μM; and 4.69 μM). In both cases,

301   background control samples were also included that lacked the presence of GDP-MP enzyme. At the

302   end of the time courses, the biochemical reactions were terminated and absorbance measurements

303   were taken. Background signal was subtracted and linear regression was performed on the

304   corresponding time versus activity plots in order to acquire relative reaction rates, which were in turn

305   used to generate classical Michaelis-Menten plots. Data were acquired from 3 independent replicates

306   (N = 3) and are represented in the figures as mean values ± SD. The K_m was obtained by fitting

307   individual replicate data to the Michaelis-Menten equation shown below:

$$v = \frac{V_{max}[\text{S}]}{K_m + [\text{S}]}$$

308

309   To measure the activity of the *T. cruzi* PMM enzyme, a PMM-GDP-MP biochemical assay system

310   was used. K_m determinations for the M-6-P substrate and G-1,6-BP co-factor were acquired as

12

311 described above by performing 60 minute time-course reactions. Fixed concentrations of PMM and

312 GDP-MP enzyme (6.25 nM and 3.13 nM, respectively), a saturating concentration of GTP (300 μM)

313 mixed with inorganic pyrophosphatase (1 U/mL), and either a saturating concentration of M-6-P (300

314 μM) or G-1,6-BP (60 μM) and varying concentrations of either G-1,6-BP (i.e. 50 μM; 25 μM; 12.5

315 μM; 6.25 μM; 3.13 μM; 1.57 μM; and 0.78 μM) or M-6-P (i.e. 800 μM; 400 μM; 200 μM; 100 μM;

316 50 μM; 25 μM; and 12.5 μM) were used. Data were acquired from 3 independent replicates (N = 3)

317 and are represented in the figures as mean values ± SD.

318

319 To confirm linearity of the GDP-MP assay in the standard and high-substrate configurations, a 50

320 minute time-course reaction was performed using either 3.13 nM or 0.78 nM of GDP-MP enzyme,

321 respectively, in the presence of M-1-P (15 μM or 150 μM), GTP (30 μM or 300 μM), and inorganic

322 pyrophosphatase (1 U/mL). In a similar manner to the above, the standard and high-substrate

323 configurations of the PMM-GDP-MP assay were tested for linearity by performing 90 minute time-

324 course reactions using 6.25 nM PMM and 3.13 nM GDP-MP enzymes in the presence of M-6-P (45

325 μM or 225 μM), G-1,6-BP (6 μM or 30 μM), GTP (150 μM), and inorganic pyrophosphatase (1

326 U/mL). In all cases, background control samples were also included that lacked the presence of

327 enzyme. At the end of the time courses, the biochemical reactions were terminated and absorbance

328 measurements were taken. Data were acquired from 4 technical replicates (N = 4) for each enzyme

329 and assay configuration, and were represented as a mean RAU values ± SD following subtraction of

330 background signal. Linear regression models were fitted to the complete data sets from the standard

331 and high-substrate configurations of the GDP-MP assay, and for the 30–90 minute and 30–80 minute

332 time frames for standard and high-substrate configurations of the PMM-GDP-MP assays respectively.

333

334 <u>DMSO tolerance.</u>

335 DMSO tolerance of the GDP-MP enzyme was investigated by incubating the enzyme (3.13 nM) in the

336 presence of GTP (30 μM), M-1-P (15 μM), inorganic pyrophosphatase (1 U/mL), and varying

13

337   volumes of DMSO (i.e. 1000 nL, 500 nL, 250 nL, 125 nL, 60 nL, and 30 nL corresponding to 2% v/v,

338   1% v/v, 0.5% v/v, 0.25% v/v, 0.12% v/v, and 0.06% v/v final assay concentrations respectively) at

339   room temperature for 60 min. DMSO was added to the assay microplate using a Preddator liquid

340   dispenser (Redd&Whyte, UK). Background control samples were also included that lacked the

341   presence of enzyme. At the end of the incubation period, the biochemical reactions were terminated

342   and absorbance measurements were taken. In a similar manner, DMSO tolerance of the PMM enzyme

343   was investigated by incubating PMM and GDP-MP enzymes (6.25 nM and 3.13 nM, respectively) in

344   the presence of GTP (150 µM), M-6-P (45 µM), G-1,6-BP (6 µM), and inorganic pyrophosphatase (1

345   U/mL). Data were acquired from 4 technical replicates (N = 4) for each enzyme, and were represented

346   as a mean RAU values + SD following subtraction of background signal.

347

348   Pyrophosphatase counter-screen assay development.

349   In order to evaluate the activity of the inorganic pyrophosphatase reporter enzyme, a 10-minute time-

350   course reaction using a fixed concentration of the enzyme (1 U/mL) and varying concentrations of

351   sodium pyrophosphate substrate (20 µM; 10 µM; 5 µM; 2.5 µM; 1.25 µM; and 0 µM) was performed.

352   Background control samples were also included that lacked the presence of pyrophosphatase enzyme.

353   At the end of the time-course, the biochemical reactions were terminated and absorbance

354   measurements were taken. Data were acquired from two technical replicates (N = 2) and were

355   represented as background subtracted RAU. To confirm the linearity of the assay, the inorganic

356   pyrophosphatase reporter enzyme (1 U/mL) was incubated at room temperature for 5 min in the

357   presence of varying concentrations of sodium pyrophosphate substrate (20 µM; 15 µM; 10 µM; 7.5

358   µM; 5 µM; 3.75 µM; 2.50 µM; 1.88 µM; 1.25 µM; and 0 µM). The colourimetric reaction was

359   developed and the data were acquired as described above. Data were obtained from 5 technical

360   replicates (N = 5), and are represented as mean RAU values ± SD following subtraction of

361   background signal. A linear regression model was fitted to the resulting plot.

362

14

363 Single-point diversity screening.

364 Single-point diversity screening was performed using the standard configuration PMM-GDP-MP

365 biochemical assay and microplates containing compounds in columns 1–22 from two diverse small-

366 molecule compound sets covering traditional small-molecule chemical space (DDD, 9,257

367 compounds; molecular weights between 185.2 and 492.2) and more three-dimensional chemical space

368 (GHCDL, 8,860 compounds; molecular weights between 190.24 and 449.3) at a final concentration of

369 10 μM (final DMSO concentration = 0.1% v/v), or a small polar set (16,845 primarily fragment-sized

370 compounds with increased polarity; molecular weights between 88.1 and 476.0) at a final

371 concentration of 300 μM (final DMSO concentration = 0.3% v/v). Columns 23 and 24 both contained

372 DMSO (either 0.1% v/v or 0.3% v/v at final assay concentration), and were utilised as 'maximum

373 effect' and 'minimum effect' control populations, respectively. For screening purposes, 25 μL of a

374 solution containing PMM and GDP-MP enzymes (6.25 nM and 3.13 nM, respectively) was added to

375 columns 1–23, and 25 μL of buffer only was added to column 24. This was followed by the addition

376 of 25 μL of a mixture containing inorganic pyrophosphatase (1 U/mL) and substrates/co-factors (150

377 μM GTP, 45 μM M-6-P, and 6 μM G-1,6,-BP). The assay plates were incubated at room temperature

378 for 90 min. At the end of the incubation period, the biochemical reactions were terminated and

379 absorbance measurements were taken. Robust Z' values were calculated for each assay microplate

380 using the following equation:

381

382 Robust Z' = 1 – ((3 x (1.483 × (RAU MAD Max)))+(3 x (1.483 × (RAU MAD Min))))/(median RAU

383 Max - median RAU Min)

384

385 where MAD = median absolute deviation; Max = maximum effect control samples; Min = minimum

386 effect control samples.

387

388 RAU values were normalised to % inhibition values relative to the maximum and minimum effect

389 control populations, and compounds displaying % inhibition values ≥30% were selected as hits. Data

390 were processed using IDBS ActivityBase 8.1.2.12 and Dotmatics Limited Vortex v2017.08.69598-59-

391 s software.

392

393

394

395 <u>Concentration-response assays</u>

396 Concentration-response assessment of hits using the PMM-GDP-MP assays was performed by adding

397 25 µL of a solution of PMM and GDP-MP enzymes (6.25 nM and 3.13 nM, respectively) to columns

398 1–11 and 13–23 of microplates containing varying concentrations of compounds (10 final assay

399 concentrations ranging from 990 µM to 1.92 µM at 1 in 3 dilution increments in the presence of 1%

400 v/v DMSO). Buffer only (25 µL) was added to columns 12 and 24. Columns 11 and 23 were utilised

401 as 'maximum effect' control populations (1% v/v DMSO with enzyme), and columns 12 and 24 were

402 'minimum effect' control populations (1% v/v DMSO in absence of enzyme). This was followed by

403 the addition of 25 µL of a mixture containing inorganic pyrophosphatase (1 U/mL) and substrates/co-

404 factors (150 µM GTP, 45 µM M-6-P, and 6 µM G-1,6-BP for the standard configuration assay, and

405 150 µM GTP, 225 µM M-6-P, and 30 µM G-1,6-BP for the high-substrate configuration assay) to the

406 entire assay plate. The standard configuration assay plates were incubated at room temperature for 90

407 min and the high-substrate configuration assay plates were incubated for 80 min. Standard and high-

408 substrate configuration GDP-MP assay compound concentration-response assessments were

409 performed as above by incubating GDP-MP enzyme (3.13 nM or 0.78 nM) in the presence of GTP

410 (30 µM or 300 µM), M-1-P (15 µM or 150 µM), and inorganic pyrophosphatase (1 U/mL) for 50 min

411 at room temperature. Pyrophosphatase counter-screen concentration-response assessments were

412 performed by pre-incubating compounds with inorganic pyrophosphatase (1 U/mL) for 90 min at

413 room temperature, followed by addition of inorganic pyrophosphate (10 µM) and a secondary 5

16

414 minute incubation at room temperature. At the end of the incubation periods, the biochemical

415 reactions were terminated and absorbance measurements were taken. RAU values were normalised to

416 % inhibition values relative to the maximum and minimum effect control populations. pIC_{50} values,

417 defined as $-\log(IC_{50} (M))$, were calculated by fitting concentration-response data for each independent

418 replicate separately to a four-parameter logistic model, as shown below, using either the IDBS

419 ActivityBase 8.1.2.12 or SigmaPlot 12.5 software. Where appropriate, the top curve plateau parameter

420 was constrained to a value of 100. Compounds requiring a concentration greater than 990 μM to

421 inhibit biochemical assay activity by at least 50% were deemed to be inactive (i.e. $pIC_{50} <3$)

422 Four-parameter logistic model:

$$y = Min + \frac{Max - Min}{1 + \left(\frac{10^{-LogIC50}}{x}\right)^{Hillslope}}$$

423 **Acknowledgements.**

427 **References.**

428 1. Andrade EV, Gollob KJ, Dutra WO. 2014. Acute chagas disease: new global challenges for an old
429 neglected disease. PLoS Negl Trop Dis 8:e3010.

430 2. Pérez-Molina JA, Molina I. 2018. Chagas disease. Lancet 391:82–94.

431 3. Urbina JA. 2015. Recent clinical trials for the etiological treatment of chronic Chagas disease:
432 advances, challenges and perspectives. J Eukaryot Microbiol 62:149–156.

433 4. Drugs for Neglected Diseases. 2017. Benznidazole new doses improved treatment and
434 associations (BENDITA). Available from: https://clinicaltrials.gov/ct2/show/study/NCT03378661.
435 ClinicalTrials.gov identifier: NCT03378661. Accessed: May 1, 2019.

436 5. Ferguson MA. 1999. The structure, biosynthesis and functions of glycosylphosphatidylinositol
437 anchors, and the contributions of trypanosome research. J Cell Sci 112:2799–2809.

438 6. Turnock DC, Ferguson MA. 2007. Sugar nucleotide pools of Trypanosoma brucei, Trypanosoma
439 cruzi, and Leishmania major. Eukaryot Cell 6:1450–1463.

17

440   7. Mucci J, Lantos AB, Buscaglia CA, Leguizamón MS, Campetella O. The Trypanosoma cruzi Surface,
441   a Nanoscale Patchwork Quilt. 2016. Trends Parasitol 33:102–112.

442   8. Pech-Canul ÁC, Monteón V, Solís-Oviedo RL. 2017. A Brief View of the Surface Membrane Proteins
443   from Trypanosoma cruzi. J Parasitol Res. 2017:3751403.

444   9. Nagamune K, Nozaki T, Maeda Y, Ohishi K, Fukuma T, Hara T, Schwarz RT, Sutterlin C, Brun R,
445   Riezman H, Kinoshita T. 2000. Critical roles of glycosylphosphatidylinositol for Trypanosoma brucei.
446   Proc Natl Acad Sci U S A 97:10336–10341.

447   10. Lillico S, Field MC, Blundell P, Coombs GH, Mottram JC. 2003. Essential roles for GPI-anchored
448   proteins in African trypanosomes revealed using mutants deficient in GPI8. Mol Biol Cell 14:1182–
449   1194.

450   11. Stokes MJ, Güther ML, Turnock DC, Prescott AR, Martin KL, Alphey MS, Ferguson MA. 2008. The
451   synthesis of UDP-N-acetylglucosamine is essential for bloodstream form trypanosoma brucei in vitro
452   and in vivo and UDP-N-acetylglucosamine starvation reveals a hierarchy in parasite protein
453   glycosylation. J Biol Chem 283:16147–16161.

454   12. Kuettel S, Wadum MC, Güther ML, Mariño K, Riemer C, Ferguson MA. 2012. The de novo and
455   salvage pathways of GDP-mannose biosynthesis are both sufficient for the growth of bloodstream-
456   form Trypanosoma brucei. Mol Microbiol 84:340–351.

457   13. Garami A, Ilg T. 2001. Disruption of mannose activation in Leishmania mexicana: GDP-mannose
458   pyrophosphorylase is required for virulence, but not for viability. EMBO J 20:3657–3666.

459   14. Garami A, Ilg T. 2001. The role of phosphomannose isomerase in Leishmania mexicana
460   glycoconjugate synthesis and virulence. J Biol Chem 276:6566–6575.

461   15. Garami A, Mehlert A, Ilg T. 2001. Glycosylation defects and virulence phenotypes of Leishmania
462   mexicana phosphomannomutase and dolicholphosphate-mannose synthase gene deletion mutants.
463   Mol Cell Biol 21:8168–8183.

464   16. Stewart J, Curtis J, Spurck TP, Ilg T, Garami A, Baldwin T, Courret N, McFadden GI, Davis A,
465   Handman E. 2005. Characterisation of a Leishmania mexicana knockout lacking guanosine
466   diphosphate-mannose pyrophosphorylase. Int J Parasitol 35:861–873.

467   17. Kedzierski L, Malby RL, Smith BJ, Perugini MA, Hodder AN, Ilg T, Colman PM, Handman E. 2006.
468   Structure of Leishmania mexicana phosphomannomutase highlights similarities with human
469   isoforms. J Mol Biol 363:215–227.

470   18. Asención Diez MD, Demonte A, Giacomelli J, Garay S, Rodrígues D, Hofmann B, Hecht HJ,
471   Guerrero SA, Iglesias AA. 2010. Functional characterization of GDP-mannose pyrophosphorylase
472   from Leptospira interrogans serovar Copenhageni. Arch Microbiol 192:103–114.

473   19. Lackovic K, Parisot JP, Sleebs N, Baell JB, Debien L, Watson KG, Curtis JM, Handman E, Street IP,
474   Kedzierski L. 2010. Inhibitors of Leishmania GDP-mannose pyrophosphorylase identified by high-
475   throughput screening of small-molecule chemical library. Antimicrob Agents Chemother 54:1712–
476   1719.

477   20. Mao W, Daligaux P, Lazar N, Ha-Duong T, Cavé C, van Tilbeurgh H, Loiseau PM, Pomel S. 2017.
478   Biochemical analysis of leishmanial and human GDP-Mannose Pyrophosphorylases and selection of
479   inhibitors as new leads. Sci Rep 7:751.

18

480   21. Edfeldt FN, Folmer RH, Breeze AL. 2011. Fragment screening to predict druggability (ligandability)
481   and lead discovery success. Drug Discov Today 16:284–287.

482   22. Zhang JH, Chung TD, Oldenburg KR. 1999. A Simple Statistical Parameter for Use in Evaluation
483   and Validation of High Throughput Screening Assays. J Biomol Screen 4:67–73.

484   23. MacLean LM, Thomas J, Lewis MD, Cotillo I, Gray DW, De Rycker M. 2018. Development of
485   Trypanosoma cruzi in vitro assays to identify compounds suitable for progression in Chagas' disease
486   drug discovery. PLoS Negl Trop Dis 12:e0006612.

487   24. Daligaux P, Bernadat G, Tran L, Cavé C, Loiseau PM, Pomel S, Ha-Duong T. 2016. Comparative
488   study of structural models of Leishmania donovani and human GDP-mannose pyrophosphorylases.
489   Eur J Med Chem 107:109–118.

490   25. Doak BC, Norton RS, Scanlon MJ. 2016. The ways and means of fragment-based drug design.
491   Pharmacol Ther 167:28–37.

492   26. Strelow J, Dewe W, Iversen PW, Brooks HB, Radding JA, McGee J, Weidner J. 2012. Mechanism
493   of Action Assays for Enzymes. In: Sittampalam GS, Coussens NP, Brimacombe K, Grossman A, Arkin
494   M, Auld D, Austin C, Baell J, Bejcek B, Caaveiro JMM, Chung TDY, Dahlin JL, Devanaryan V, Foley TL,
495   Glicksman M, Hall MD, Haas JV, Inglese J, Iversen PW, Kahl SD, Kales SC, Lal-Nag M, Li Z, McGee J,
496   McManus O, Riss T, Trask OJ Jr., Weidner JR, Wildey MJ, Xia M, Xu X, editors. Assay Guidance Manual
497   [Internet]. (MD): Eli Lilly & Company and the National Center for Advancing Translational Sciences.
498   2004-. Available from: https://www.ncbi.nlm.nih.gov/books/NBK92001/

499   **Figures.**

500

501   Figure 1. The GDP-Man biosynthetic pathway in *T. cruzi*. Glc = glucose; G-6-P = glucose-6-

502   phosphate; G6PI = glucose-6-phosphate isomerase; F-6-P = fructose-6-phosphate; PMI =

503   phosphomannose isomerase; M-6-P = mannose-6-phosphate; PMM = phosphomannomutase; G-1,6-

504   BP = glucose-1,6-bisphosphate; M-1-P = mannose-1-phosphate; GDP-MP = guanosine diphosphate-

505   mannose pyrophosphorylase; GTP = guanosine triphosphate; GDP-Man = guanosine diphosphate-

506   mannose; GIPLs = glycosylinositol phospholipids; and GPI = glycosylphosphatidylinasitol.

507

508   Figure 2. The biochemical assay platforms. M-6-P = mannose-6-phosphate; PMM =

509   phosphomannomutase; G-1,6-BP = glucose-1,6-bisphosphate; M-1-P = mannose-1-phosphate; GDP-

510   MP = guanosine diphosphate-mannose pyrophosphorylase; GTP = guanosine triphosphate; GDP-Man

511   = guanosine diphosphate-mannose; PPiase = pyrophosphatase.

512

513   Figure 3. Michaelis-Menten plots for M-1-P (a) and GTP (b) substrates of the *T. cruzi* GDP-MP

514   enzyme obtained using the GDP-MP biochemical assay, and the M-6-P substrate (c) and G-1,6-BP

515   co-factor (d) of the *T. cruzi* PMM enzyme obtained using the PMM-GDP-MP biochemical assay.

516   Data represents mean of three independent replicates (N = 3). Error bars represent ± SD.

517

518

519

520

20

521 Table 1. K_m parameters for the *T. cruzi* GDP-MP substrates M-1-P and GTP, and the *T. cruzi* PMM

522 substrate M-6-P and the co-factor G-1,6-BP, and the substrate and co-factor concentrations that were

523 chosen for screening using the standard and high-substrate assay configurations.

| K_m determinations | | | Screening conditions, μM | | | |
| | | | Standard configuration | | High-substrate configuration | |
Substrate	K_m, μM[a]	95% CI, μM	GDP-MP	PMM-GDP-MP	GDP-MP	PMM-GDP-MP
M-1-P	13.3	12.8–13.8	15	-	150	-
GTP	40.7	31.9–51.6	30	150	300	150
M-6-P	48.2	44.3–52.4	-	45	-	225
G-1,6-BP	7.8	6.4–9.5	-	6	-	30

524 [a]Data represents mean of three independent replicates (N = 3).

525

526 Figure 4. (a) Single point screen of 18,117 compounds at a concentration of 10 μM from two diversity

527 compound sets and (b) single point screen of 16,845 compounds at a concentration of 300 μM from a

528 small polar fragment set using the standard configuration *T. cruzi* PMM-GDP-MP biochemical assay.

529 Red circles represent compounds exhibiting ≥30% inhibition. Interfering compounds exhibiting <-

530 100% inhibition were removed.

531

532 Figure 5. Plots showing the linear correlations between pIC$_{50}$ values of 46 hit compounds obtained for

533 two independent replicate datasets acquired using (a) the standard configuration *T. cruzi* PMM-GDP-

534 MP biochemical assay ($R^2 = 0.98$) and (b) the reporter technology interference counter-screen assay

535 ($R^2 = 0.93$). (c) A plot of the mean pIC$_{50}$ values (N = 2) for the hit compounds obtained using the

536 standard configuration *T. cruzi* PMM-GDP-MP biochemical assay versus the reporter technology

537 interference counter-screen assay. Red triangles represent 20 compounds that were active against the

538 former assay (pIC$_{50}$ ≥3) and inactive against the counter-screen assay (pIC$_{50}$ <3).
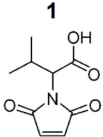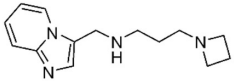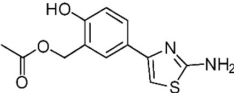
539

21
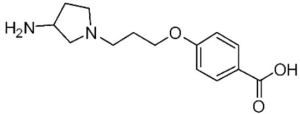
540   Figure 6. A plot showing the linear correlation ($R^2 = 0.81$) between the mean pIC_{50} values (N = 2) of

541   the 20 hit compounds obtained using the standard configuration *T. cruzi* PMM-GDP-MP assay versus

542   the pIC_{50} values (N = 1) obtained using the standard configuration *T. cruzi* GDP-MP assay.

543

544   Table 2. Structures and pIC_{50} parameters of the four most potent compounds (i.e. compounds **1**–**4**)

545   acquired using the standard- and high-substrate configuration *T. cruzi* PMM-GDP-MP and GDP-MP

546   assays.

547

548   [a]SC = standard configuration; [b]HSC = high-substrate configuration; [c]acquired using library stock

549   material; [d]acquired using re-purchased material. Mean pIC_{50} parameter values are reported where N

550   ≥ 2. Compounds with a $pIC_{50} < 3.0$ were deemed inactive in the corresponding biochemical assay.

22

Compound	Assay	pIC50[c] (N)	pIC$_{50}$[d] ± SD (N)
1	PMM-GDP-MP, SC[a]	4.9 (2)	-
	PMM-GDP-MP, HSC[b]	-	-
	GDP-MP, SC[a]	4.6 (1)	-
	GDP-MP, HSC[b]	-	-
2	PMM-GDP-MP, SC[a]	3.6 (2)	3.1 ± 0.2 (3)
	PMM-GDP-MP, HSC[b]	-	3.2 ± 0.2 (3)
	GDP-MP, SC[a]	<3.0 (1)	<3.0 (3)
	GDP-MP, HSC[b]	-	3.1 ± 0.1 (3)
3	PMM-GDP-MP, SC[a]	3.5 (2)	3.9 ± 0.2 (3)
	PMM-GDP-MP, HSC[b]	-	3.6 ± 0.1 (3)
	GDP-MP, SC[a]	3.8 (1)	3.9 ± 0.1 (3)
	GDP-MP, HSC[b]	-	3.5 ± 0.1 (3)
4	PMM-GDP-MP, SC[a]	4.0 (2)	-
	PMM-GDP-MP, HSC[b]	-	-
	GDP-MP, SC[a]	3.8 (1)	-
	GDP-MP, HSC[b]	-	-

Hexokinase	G6PI	PMI	PMM	GDP-MP

Glc $\longrightarrow$ G-6-P $\rightleftharpoons$ F-6-P $\rightleftharpoons$ M-6-P $\rightleftharpoons$ M-1-P $\rightleftharpoons$ GDP-Man $\longrightarrow$ GIPLs / GPI anchors / N-glycans

G-1,6-BP   GTP

GDP-MP assay

<u>Standard configuration:</u> M-1-P and GTP at approx. K_m

<u>High-substrate configuration:</u> M-1-P and GTP at approx.10-fold K_m

Pyrophosphatase counter-screen assay

| PMM | | GDP-MP | | PPiase |

G-1,6-BP   GTP   BIOMOL® Green

M-6-P ⇌ M-1-P ⇌ GDP-Man + $P_2O_7^{2-}$ ⟶ $2\ PO_4^-$ ⟶ Colourimetric read out

PMM-GDP-MP assay

<u>Standard configuration:</u> M-6-P and G-1,6-BP at approx. K_m, and GTP at approx. 5-fold K_m

<u>High-substrate configuration:</u> M-6-P, G-1,6-BP, and GTP at approx. 5-fold K_m

a.

b.

c.

d.

a.

b.

a.

b.

c.